INTERACTION BETWEEN SOIL HYDROLOGY AND BOUNDARY-LAYER DEVELOPMENT

H.-L. PAN and L. MAHRT

Department of Atmospheric Sciences, Oregon State University, Corvallis, OR 97331, U.S.A.

(Received in final form 31 October, 1986)

Abstract. A two-layer model of soil hydrology and thermodynamics is combined with a one-dimensional model of the planetary boundary layer to study various interactions between evolution of the boundary layer and soil moisture transport. Boundary-layer moistening through surface evaporation reduces the potential and actual surface evaporation as well as the boundary-layer growth. With more advanced stages of soil drying, the restricted surface evaporation allows greater sensible heat flux which enhances boundary-layer growth and entrainment drying.

Special individual cases are studied where the wind speed is strong, solar radiation is reduced, transpiration is important, the soil is thin, or the soil is covered with organic debris.

1. Introduction

Surface evaporation can substantially reduce surface heating and subsequent development of the daytime boundary layer. As a result, boundary-layer development is quite sensitive to availability of surface moisture as previously demonstrated by McCumber and Pielke (1981).

The interaction among surface evaporation, soil moisture and boundary-layer development is quite complex even in the cloudless case as noted schematically in Figure 1. For example, the reduction of boundary-layer development is partially limited by negative feedbacks. As surface evaporation moistens the boundary layer, the potential evaporation normally decreases, which in turn reduces the actual evaporation. Exceptions include the case of strong downward entrainment of drier air where low humidities are maintained in spite of significant evaporation.

On a longer time scale, the surface evaporation may significantly deplete the soil moisture. This drying reduces the surface evaporation even though it also acts to increase the potential evaporation. The time-scale for this process depends on soil properties as well as atmospheric conditions.

Suitable observations which include both adequate measurements of soil variables and atmospheric fluxes are not available to study the various stages of drying. In this paper we use a relatively simple model of the soil-atmosphere system to identify the importance of various interactions related to surface evaporation. The results of this study or any modelling effort will remain necessarily inconclusive until the required measurements become available. Our goal is to suggest the most important interactions. Such information can assist in the design of future observational programs as well as help identify the most critical parts of the soil-atmospheric modelling.

Boundary-Layer Meteorology **38** (1987) 185–202.

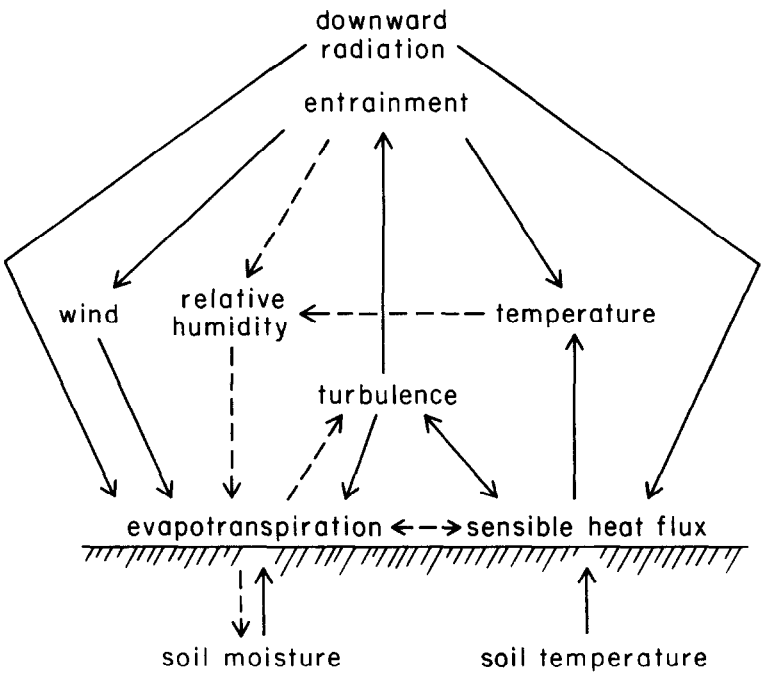

Fig. 1. Suspected important interactions between surface evapotranspiration and boundary-layer development for conditions of daytime surface heating. Solid arrows indicate the direction of feedbacks which are normally positive (leading to increases of the recipient variable). Broken arrows indicate negative feedbacks. Two consecutive negative feedbacks make a positive one.

A second goal of this work is to provide a soil-atmosphere boundary layer model which is sufficiently simple to use in concert with larger scale atmospheric models. Recent numerical experiments by Hunt (1985) indicate that formulations for soil moisture and surface evaporation presently used in general circulation models have serious shortcomings. The present formulation is somewhat more complicated but physically more direct.

2. The Model

The atmospheric boundary-layer model of Troen and Mahrt (1986) is coupled to the soil moisture model of Mahrt and Pan (1984). The atmospheric model contains 34 levels between the surface and 4 km, although approximately the same results can be obtained with as few as 10 levels. The boundary-layer height in the model is determined using a diagnostic relationship based on a modified bulk-Richardson number at each time step. During the day, the boundary layer grows in response to turbulence generated by surface heating. When the solar radiation vanishes and if winds are weak, the boundary layer normally collapses to the first model layer (~ 50 m).

The soil model consists of a thin upper layer, 5 cm thick, which responds mainly to diurnal variations, and a thicker lower layer, 95 cm thick, which participates more in seasonal changes of soil water storage. The potential evaporation is formulated with a modified Penman relationship (Mahrt and Ek, 1984). The finite differencing of the soil model has been chosen to minimize truncation errors. This choice is based on comparisons with higher resolution versions of the model up to 100 layers. The truncation errors for the two-layer model, compared to higher resolution versions, led to overestimation of the evaporation of about 10% for the case of clay soil and only a few percent for the case of sand. These errors are small compared to other uncertainties such as treatment of the soil-air interface. Because an accurate description of moisture transport close to the soil surface requires prohibitive vertical resolution, the modelled surface moisture flux is substantially overestimated and is compensated by increasing the air-dry values for the soil moisture content to 0.16 and 0.25 for sand and clay, respectively. A 10-min time step is used in all model runs.

The soil model of Mahrt and Pan (1984) has been generalized to include soil heat flux using the usual thermodynamic relationship:

$$C \frac{\partial T}{\partial t} = \frac{\partial}{\partial z}\left(K \frac{\partial T}{\partial z}\right)$$

where the volumetric heat capacity C and the thermal conductivity K are formulated as functions of soil water content as in McCumber and Pielke (1981). A more detailed discussion of the soil-thermodynamic model is given in Appendix A.

The soil drying period, and feedback to the atmosphere, usually extend over several days or even several weeks. Iteration of one-dimensional models for such periods leads to unrealistic buildup of moisture and heat. This buildup does not occur in the atmosphere because of clear-air radiative cooling, horizontal advection of heat and moisture, and consumption of moisture by precipitating systems. Such processes cannot be sensibly formulated within the present framework; instead we specify a climatic advection or restoring term of the form

$$(q_E - q)/\tau_q\,, \qquad (\theta_E - \theta)/\tau_\theta\,,$$

where q and θ are the actual values of specific humidity and temperature, and q_E and θ_E are pseudo-equilibrium values. In the present study q_E is specified to be the initial conditions described below, while θ_E is specified to be height-independent with a value of 270 K. Heat buildup was controlled by specifying a relaxation time of $\tau_\theta = 10$ days while long-term moisture buildup was prevented with a shorter relaxation time of $\tau_q = 1$ day. While advection is pragmatically specified in this modelling study, it is also thought to exert a controlling influence on evaporation, at least in some flow situations (McNaughton, 1976).

The atmospheric temperature is initialized with a constant lapse rate (6 K km^{-1}). The temperature at the lowest atmospheric model-level is initialized at 283.6 K. The initial moisture content of the atmosphere is specified to be 3 g kg^{-1} in the lowest

kilometer, 2 g kg^{-1} between 1 and 1.2 km, 1 g kg^{-1} between 1.2 km and 2 km, and 0.5 g kg^{-1} above 2 km. Both the initial wind and the time-independent geostrophic wind are specified to be 5 m s^{-1}. The initial volumetric moisture content of the soil is specified to be 0.42, a value which is saturated with respect to clay and super-saturated with respect to sand, leading to large percolation through the bottom of the sand for the first day. The initial soil temperature is specified to be identical to the initial value at the lowest atmospheric level (283.6 K).

The short-wave radiative flux formulation of Holtslag and Van Ulden (1983) is applied for 45 °N starting with 21 June. Albedo for the Earth's surface is set at 0.25. For simplicity, we neglect the change of soil surface albedo with soil drying which can lead to significant decreases of potential evaporation (Van Bavel and Hillel, 1976). Downward long-wave radiative flux is assumed to be constant corresponding to a black-body temperature of 270 K. Each numerical experiment is iterated for 21 days in order to include the important evaporation stages.

In the next section, four prototype numerical experiments are iterated for sand and clay soil types and for geostrophic wind speeds of 5 or 10 m s^{-1}.

3. Drying Stages

Radiative fluxes, wind speed, moisture deficit, and atmospheric stability determine the potential evaporation, which in turn forces the actual soil evaporation. When the soil is relatively wet, evaporation will be at the potential rate (atmospheric demand) as determined by atmospheric conditions. When the soil is sufficiently dry, the rate of evaporation is controlled by the soil moisture gradient in the upper part of the soil. The various atmospheric influences on the potential evaporation interact with soil moisture in a nonlinear fashion. Some of the candidate interactions are noted in Figure 1.

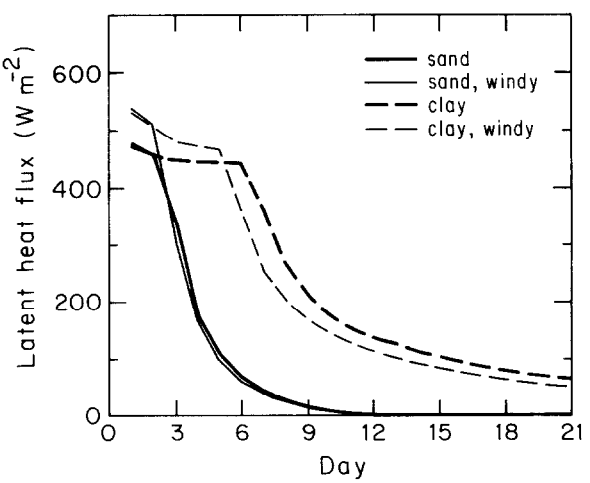

Fig. 2. The evolution of the noontime surface evaporation for clay and sand for modest geostrophic winds of 5 ms^{-1} and strong geostrophic winds of 10 ms^{-1}.

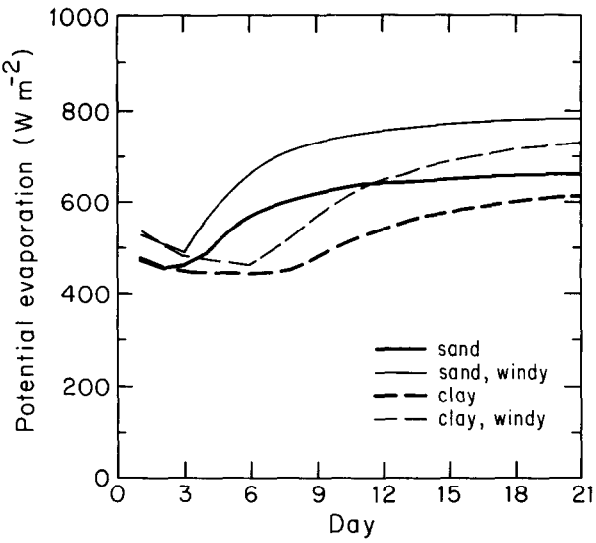

Fig. 3. Evolution of the noontime potential evaporation.

We first study the various stages of drying occurring during 21-day iterations by plotting the solar noon values of different variables over sand and clay soils for the two different values of the geostrophic wind speed. Since vegetation, clouds and precipitation are not included, extensive drying and warming will result.

The soil drying and long-term boundary-layer changes can be divided into three main stages. In the first stage, the surface evaporation is at the potential rate, which decreases slightly with time (Figures 2 and 3). In the second stage, the actual evaporation decreases rapidly with time while the potential evaporation increases with time. The second stage leads to a near-equilibrium third stage where the evaporation and potential evaporation vary slowly with time. The evolution proceeds more rapidly with sandy soil, partly because sand has a larger hydraulic diffusivity and conductivity at high volumetric water content and therefore loses more water to percolation. The stages of drying corresponding to Figures 2 and 3 are similar to those in the modelling study of Van Bavel and Hillel (1976) except that they included the dependence of surface albedo on soil wetness and neglected adjustment of the atmosphere to surface evaporation.

3.1. First stage: potential evaporation

During the first stage when evaporation is at the potential rate, both the specific humidity and the relative humidity increase with time (Figure 4) leading to a modest decrease of the potential evaporation. In most previous modelling studies of the drying stages, the potential evaporation is held constant. The slight decrease of temperature (not shown) and the corresponding decrease of saturation vapor pressure also cause the potential evaporation to decrease during the first stage. As a result of decreased evaporation, the surface sensible heat flux to the atmosphere increases during this period (not shown) even though the surface temperature decreases.

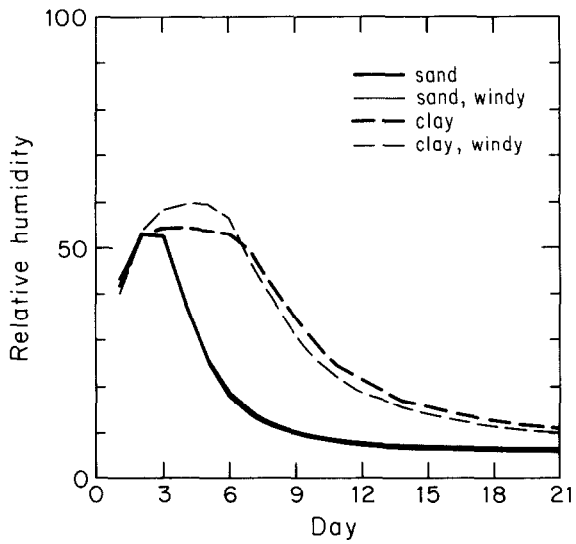

Fig. 4. Evolution of the noontime relative humidity at 50 m.

The boundary layer grows deeper (Figure 5) each subsequent day partly due to the increase of sensible heat flux. Part of the increase is due to the fact that the boundary layer grows quickly through the weakly stratified layer remaining from the mixed layer of the previous day.

The wind speed significantly influences the surface heat budget and boundary-layer evolution during the first stage of drying since the surface evaporation is at the potential

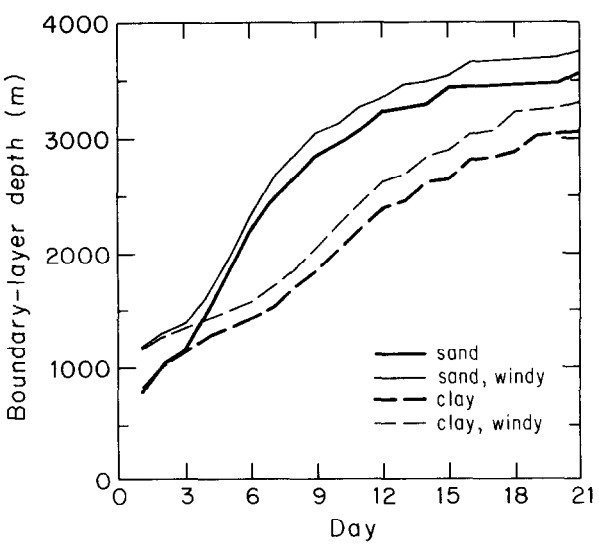

Fig. 5. Evolution of the noontime boundary-layer depth.

rate, which depends on the wind speed. On the other hand, the soil type is of little importance since the evaporation is determined completely by the atmospheric demand during this stage.

3.2. Second Stage: Rapid Decrease of Evaporation

The onset of the second stage of drying is determined by the soil type. The clay soil is able to meet the potential evaporation for five or six days while for sand, the evaporation falls significantly below the potential rate during the third day. With the onset of the

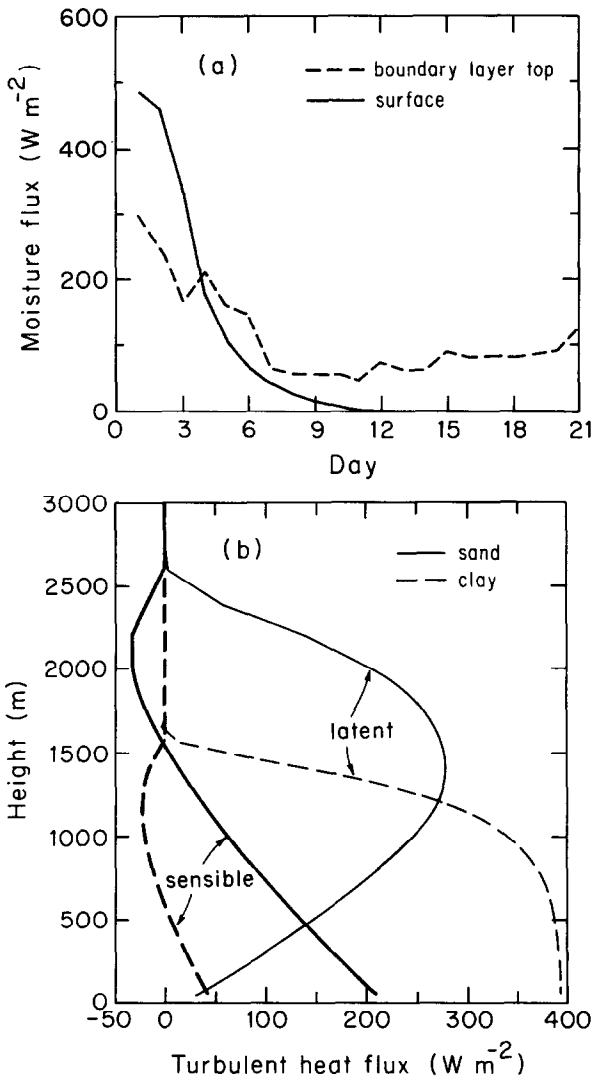

Fig. 6. (a) Evolution of the surface moisture flux and the moisture flux near the boundary-layer top over sandy soil with a geostrophic wind speed of 5 ms^{-1}. (b) Vertical profiles of the heat and moisture fluxes at 1000 hr on day 8 with a geostrophic wind speed of 5 ms^{-1}.

second stage of drying, the evaporation depends mainly on soil type and is less dependent upon wind speed and other atmospheric properties.

At the same time, atmospheric conditions change rapidly at the beginning of the second stage of drying. The decreasing surface evaporation causes a sharp increase of the surface temperature, which in turn increases the surface heat flux and boundary-layer growth. Of special importance is that the downward entrainment of drier air from above the boundary layer can exceed the surface evaporation (Figure 6a) leading to divergence of the upward moisture flux. This causes drying of the boundary layer. As expected, this net drying occurs first over sandy soil. Entrainment drying is encouraged by the relatively dry air aloft. Entrainment drying is thought to be frequently important in the evolution of high-plains boundary layers where air above the boundary layer is often dry (Mahrt, 1976). In contrast, with weaker boundary-layer growth and more humid air aloft, the entrainment drying is relatively unimportant (DeBruin, 1983).

The warming and drying cause the relative humidity to decrease and the potential evaporation to increase. However, because of increasing control of evaporation by the drying soil, the actual evaporation decreases rapidly during stage two. The decrease of surface evaporation during stage two causes major changes in the development and structure of the boundary layer. For example, consider the atmosphere profiles at 1000 solar time on day 8 (Figure 6b). Over sandy soil, the surface evaporation is already quite small, leading to large surface heat flux and vertical profiles of the heat flux typical of the convective mixed layer. The heat flux decreases linearly with height, reaching negative values near the boundary-layer top due to downward entrainment of warmer air.

In contrast, surface evaporation over the clay soil is still relatively large leading to smaller surface heating and thinner boundary-layer depth. The upper two-thirds of the boundary layer is characterized by downward heat flux associated with entrainment. This implies that during this period, the mixing in the boundary layer over clay is driven primarily by mean shear whereas mixing in the boundary layer over sand is primarily driven by convection. This example shows how boundary-layer development depends on soil type through the role of surface evaporation.

3.3. Stage three: near-equilibrium

Eventually the boundary layer approaches an equilibrium state characterized by warm and dry conditions. At noon the surface evaporation becomes negligible for sand and less than 10% of the potential rate over the clay soil. The boundary layer is deep, exceeding 4 km for sand. At this stage of development, the depth of real boundary layers would normally be constrained by synoptic or cloud-induced subsidence and/or advection of smaller boundary-layer depth while some surface evaporation would be maintained by vapor transport in the soil and perhaps transpiration, all of which are neglected in these numerical experiments.

4. Transpiration

Realistic modelling of interaction between the soil and the atmospheric boundary layer must include the influence of the vegetative canopy. Vegetation moderates diurnal variations. Furthermore, the difference between the three stages of drying are not as distinct since the vegetation removes water from the deeper root zone which dries only slowly. Here the root zone is specified to extend to the bottom of the 1 m layer. With deep rooted plants, the influence of rapid drying of the soil surface is then less important.

We formulate the influence of the vegetative canopy in the simplest possible way which approximates the most important aspects of the canopy; namely, transpiration and shading of the soil surface. These formulations are detailed in Appendix B.

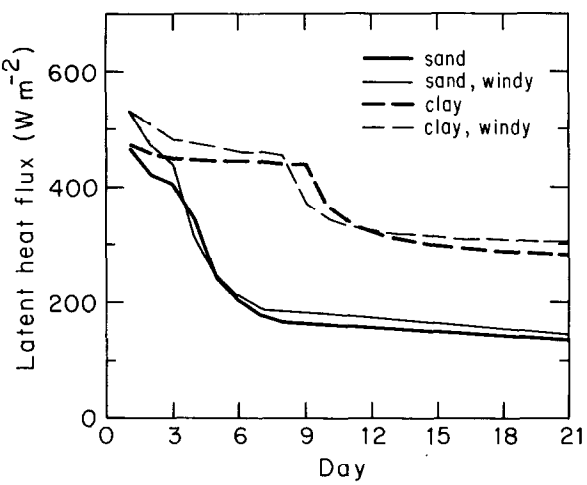

Fig. 7. Evolution of noontime evaporation for the case of surface transpiration as compared to the standard case with no transpiration.

With other conditions the same as in Section 3, the presence of the canopy shading 70% of the ground extends the period of evaporation at the potential rate by several days for clay (Figure 7); less soil water is removed from near the soil surface to meet the atmospheric demand. The decrease of evapotranspiration during stage two is less, compared to the case of no canopy. In other terms, drying of the soil surface does not substantially reduce the transpiration rate in that significant transpiration of deep soil water is maintained during stages 2 and 3. As a further result of the transpiration, the boundary layer is cooler, more moist and not as deep compared to the case with no vegetation. A fourth stage where transpiration decreases due to depletion of deep soil moisture was not studied here.

5. Influence of Solar Radiation, Climatic Advection, and Soil Properties

It is instructive to study the sensitivity of the above conclusions to variations of the external forcing. This is most simply carried out by neglecting the canopy. We first examine the winter case (solstice) where the incoming solar radiation is much reduced. Under such conditions, the drying stages evolve more slowly (Figure 8a) due to much lower rates of potential evaporation. The second stage of drying with sand does not begin until after one week, while the evaporation from the clay soil remains near the potential rate during the entire 21-day period of numerical integration. The potential evaporation reaches only about $100\ \mathrm{W\ m^{-2}}$ during mid-day so that transport of moisture within the clay soil is able to meet the demand. During the night, vertical transport within the clay is able to restore the soil moisture near the surface to the extent that the evaporation is near potential during the subsequent daytime period.

In actual atmospheric conditions, advection of heat and moisture can significantly alter the boundary-layer evolution even on short time-scales. Here we study the influence of advection as formulated in Section 2 for the summertime case. With less dry-air advection, the boundary layer moistens, which reduces the potential evaporation and significantly delays the transition to the second stage of drying for clay, as is evident in Figure 8b, for the case where the relaxation time for moisture is increased to 10 days. With reduced cold-air advection (not shown), the boundary layer heats up and grows faster, which in turn increases the downward flux of dry air.

When the soil is thinner, it stores less moisture. As a result, the second stage of drying begins slightly earlier. As an example, decreasing the soil depth from 1 to $\frac{1}{2}$ m advances onset of the second stage of drying by only a day or less, depending on soil type (Figure 8c). However, the influence of thinner soil becomes more significant at later times when the moisture content of the thin soil decreases to near air-dry values. The surface evaporation rates at stages 2 and 3 are only a fraction of the corresponding values for a 1 m thick soil.

Often natural surfaces are covered by organic 'debris' or 'litter' consisting of dead grass and leaves, conifer needles and other organic matter. Such materials cover a major portion of natural land surfaces. When dry, these materials are characterized by extremely low hydraulic conductivities; such surfaces then act as a moisture barrier and the soil becomes decoupled from the atmosphere on short time-scales in cases with little transpiration.

The thermal and hydraulic properties of such organic debris are not well known. Better known are the properties of peat soils, which are between those properties of organic surface material and those of other soils. In this study, we use the thermal and hydraulic properties for peat adopted by McCumber and Pielke (1981). The saturation water content for peat is nearly twice that of the other soil types. The hydraulic conductivity coefficient of saturated peat is similar to that of other soil types at or near saturation. However, as soil moisture decreases, the hydraulic conductivity for peat decreases rapidly to values several orders of magnitude smaller at water contents comparable to the saturation values of sand and clay. At this stage, the peat becomes

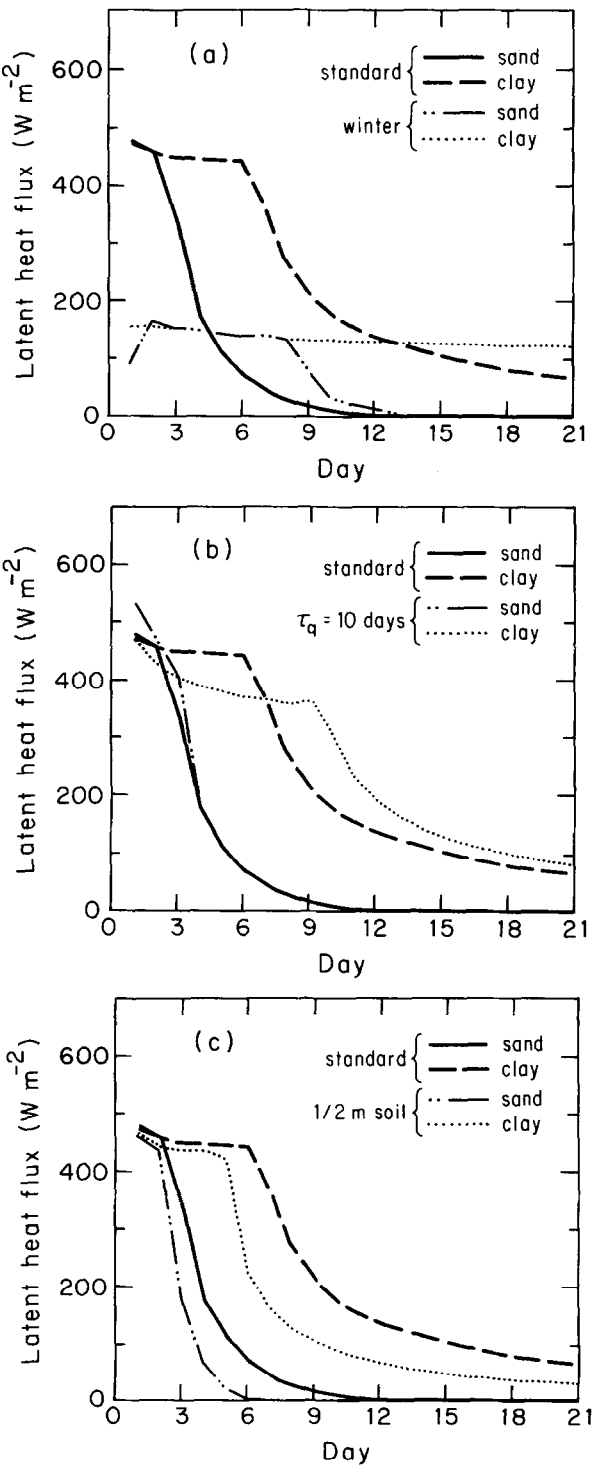

Fig. 8. The noontime surface evaporation for the special cases of (a) winter solstice sun angle, (b) reduced dry-air advection, and (c) thin soil depth, all compared to the standard case.

an effective moisture barrier which eliminates direct exchange between the soil and atmosphere.

Several numerical iterations were performed where the upper 5 cm was specified to be peat (not shown). The contribution of the surface evaporation to the surface energy balance quickly becomes negligible. In any event, the usual neglect of organic litter in large-scale modelling studies probably leads to significant overestimation of evaporation from the soil over vegetated natural surfaces. Results are only useful qualitatively since the interface between the organic material and the more conventional soil cannot be modelled with certainty. Furthermore, organic litter can reduce run-off by absorbing more rain water. This can actually lead to increased evaporation at a later stage during near-drought conditions.

6. Diurnal Variation

As an example, the diurnal variation of the surface energy budget is shown in Figure 9 for the standard case with sandy soil during days 3 and 4, which corresponds to the beginning of the second stage of soil drying. Note that on day 4, the evaporation is significantly reduced, leading to greater sensible heat flux to the atmosphere.

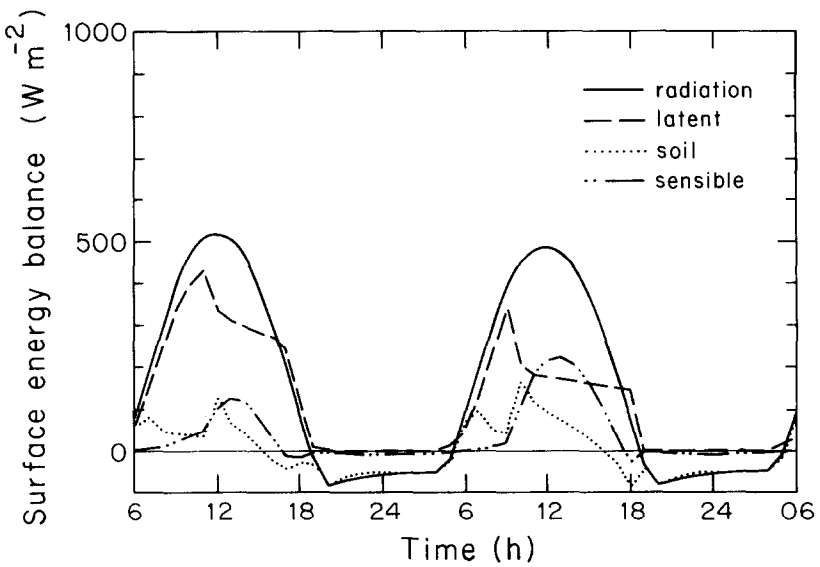

Fig. 9. The diurnal variation of the surface energy balance over sand with a geostrophic wind of 5 ms^{-1}. Positive net radiation corresponds to a net heat gain at the surface while positive values of the other terms correspond to a heat flux away from the surface.

The surface evaporation increases during the morning as dictated by increasing net radiation and resulting increase of potential evaporation (Figure 9). This rapid increase of evaporation suppresses sensible heat flux to the atmosphere and leads to temporary

retardation of heat flux to the soil. By late morning, the soil surface layer has dried to the extent that the evaporation becomes subpotential and decreases in an absolute sense. With less evaporation, the sensible heat flux to the atmosphere increases rapidly and more heat is transported into the soil. Note that the heat flux to the soil peaks earlier than the sensible heat flux to the atmosphere, since the soil warms more rapidly than the atmosphere. The delay of the diurnal increase of sensible heat flux to the atmosphere is often observed (e.g., Oke, 1978).

7. Conclusions

In the above modelling study, the soil drying advances in three stages as has been previously observed. In the first stage, the rate of surface evaporation proceeds at the potential rate and, therefore, depends mainly on atmospheric conditions such as wind speed, relative humidity, and incoming solar radiation. Surface heating is limited by the surface evaporation, and the boundary layer may develop primarily due to shear. In such cases, weak entrainment heat flux can extend downward through much of the boundary layer. In the second stage, the evaporation decreases rapidly to well-below potential values and becomes controlled more by the moisture gradients in the soil. In the final stage, the drying reaches a small near-equilibrium value. The surface heat flux becomes much larger than the latent heat flux and upward heat flux extends upward to the entrainment region of the boundary-layer top.

The duration of each stage depends critically on the soil type as well as on atmospheric conditions. The occurrence of dry organic debris, such as leaves and dead grass, appears to partially decouple the atmosphere and soil, resulting in significant slowing of the advance of the second and third stages. The development of significant transpiration reduces the importance of direct surface evaporation from the soil and thus reduces the distinction between the three stages. Entrainment drying of the boundary layer can become important with dry air aloft and strong surface heating. The latter is encouraged by dry soil conditions.

Climatic cooling and drying was specified to simulate advection, clear air radiative cooling and removal of moisture by convective clouds. Such mechanism are not necessary when simulating only one diurnal cycle or when the one-dimensional model is combined with a larger scale model. We are presently using the boundary-layer soil model with the global spectral model of Brenner *et al.* (1984).

Acknowledgements

The authors gratefully acknowledge the helpful comments of Stuart Childs of the Soil Science Department at Oregon State University. This work was supported by Contract No. F19628–84–K–0044 from AFGL, Cambridge, MA, U.S.A. Computational assistance provided by Mr Wayne Gibson is gratefully appreciated.

Appendix A: The Two-Layer Soil Thermodynamic Model

The two-layer structure used for the soil moisture model (Mahrt and Pan, 1984) should adequately resolve the diurnal variation of the soil thermodynamics; the thin top layer with a thickness of 5 cm can provide an estimate of the sharp diurnal thermal gradient and the thicker second layer (95 cm) allows us to incorporate heat storage and seasonal variations and to specify a constant lower-boundary soil temperature which, in reality, varies on the annual time-scale.

The heat conduction equation, neglecting horizontal interactions, is given as

$$C \frac{\partial T}{\partial t} = \frac{\partial}{\partial z}\left(K \frac{\partial T}{\partial z}\right), \tag{A-1}$$

where C is the volumetric heat capacity and K is the thermal conductivity. The heat capacity for water is $4.2 \times 10^6\ \mathrm{W\,m^{-3}\,K^{-1}}$ and for soil is chosen as $1.26 \times 10^6\ \mathrm{W\,m^{-3}\,K^{-1}}$ for simplicity even though it varies slightly for different soil types. The heat capacity of the composite soil is simply defined as

$$C = (1 - \theta)C_{\text{soil}} + \theta C_{\text{water}},$$

where θ is the volumetric water content. In this definition, we have neglected the contribution due to air, following DeVries (1975). The thermal conductivity, K, is strongly dependent on the soil moisture content. Similar to McCumber and Pielke (1981), we also adopted the functional form for K following A1 Nakshabandi and Kohnke (1965):

$$K(\theta) = \begin{cases} 420 \exp(-P_f + 2.7), & P_f \leq 5.1, \\ 0.1722, & P_f > 5.1; \end{cases} \tag{A-2}$$

where $P_f = \log_{10}[\psi_s(\theta s/\theta)^b]$. The factors ψ_s, θ_s, and b are functions of the soil textural class (Clapp and Hornberger, 1978).

In the finite difference formulation, the model equation (A-1) will be integrated first over the two layers to express the flux $K\,\partial T/\partial z$ explicitly, through each layer. The model grid staggering is presented in Figure A1, the level $\tilde{z}_k$ represents the level along which the temperature T_k is the same as the layer-average T (in this study, the mid-point of the layer is selected). The layer-integrated equation becomes

$$C(\tilde{\theta}_k) \frac{\partial \tilde{T}_k}{\partial t} = \frac{1}{\Delta z_k}\left[K(\theta_{k-1}) \left.\frac{\partial T}{\partial z}\right|_{z_{k-1}} - K(\theta_k) \left.\frac{\partial T}{\partial z}\right|_{z_k}\right] \tag{A-3}$$

where the gradient $\partial T/\partial z$ is evaluated as

$$\left.\frac{\partial T}{\partial z}\right|_{z_k} = \frac{\tilde{T}_k - \tilde{T}_{K+1}}{(\Delta \tilde{z})_k}. \tag{A-4}$$

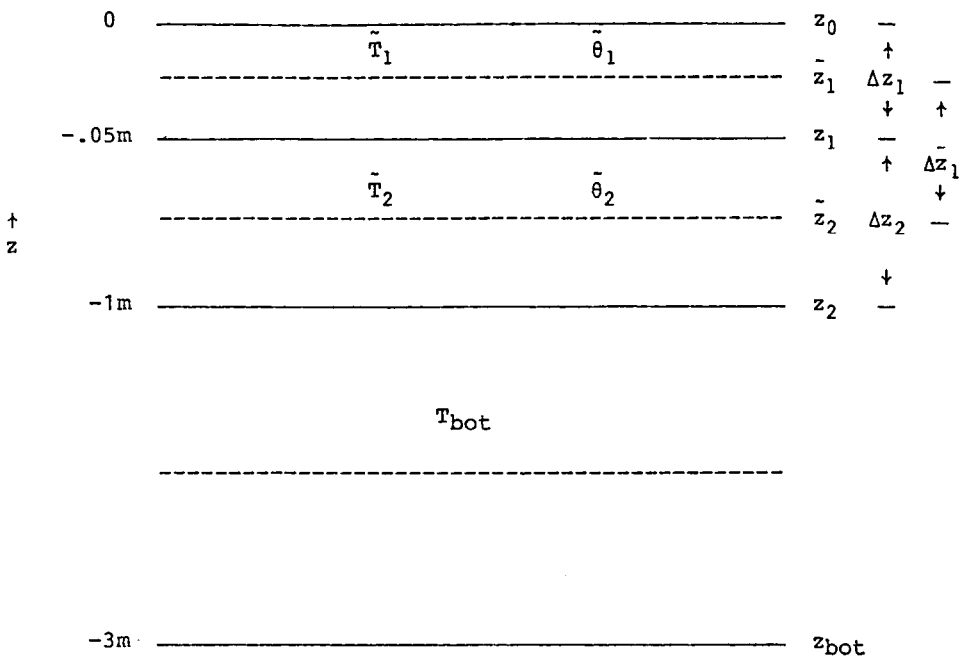

Fig. A-1. The geometry of the soil thermodynamics.

At the top of the model, the surface temperature T_s will be used to form a one-sided estimate of the gradient

$$\left.\frac{\partial T}{\partial z}\right|_{z_0} = \frac{\tilde{T}_s - \tilde{T}_1}{0.5\Delta z_1} \,. \tag{A-5}$$

The gradient at the bottom of the model is estimated using a specified constant temperature, T_{bot} (Figure A1).

In order to interface the soil thermodynamics into the model, the prediction of $\tilde{T}_k$ using (A-3) is performed using the fully implicit Cranck–Nicholson scheme given by

$$\tilde{T}_k^{(n+1)} - \tilde{T}_k^{(n)} = \frac{\Delta T}{C(\tilde{\theta}_k)} \frac{1}{(\Delta z)_k} \left[K(\theta_{k-1}) \left.\frac{\partial T^{(n+1)}}{\partial z}\right|_{z_{k-1}} - K(\theta_k) \left.\frac{\partial T^{(n+1)}}{\partial z}\right|_{z_k} \right], \tag{A-6}$$

where the superscripts designate the time levels.

For moist soil, a small difference in the thermal gradient in (A-5) can lead to large soil heat flux because the thermal conductivity increases rapidly with soil moisture content. For this reason, the surface energy balance equation must be updated simultaneously with the soil thermodynamic equations so that the resulting surface temperature and soil temperature satisfy the surface energy balance constraint at the next time step.

Appendix B: Transpiration

This appendix describes the transpiration formulation for the results in Section 4. We want to preserve the distinction since the direct soil evaporation is most appropriately related to the soil moisture of an upper thin layer while water for transpiration originates more from the deeper root zone. The total evaporation can be written as

$$E = E_{\text{dir}} + E_T + E_C\,, \tag{B-1}$$

where E_{dir} is the direct evaporation from the soil, E_T is the transpiration, and E_C is the evaporation of precipitation intercepted by the canopy. Each of the evaporation terms on the right-hand side are proportional to the potential evaporation E_P (we do not differentiate between ground temperature and 'leaf' temperature in this study).

Vegetation reduces the direct evaporation from the soil by shading the ground and reducing the wind speed near the ground. The reduction of wind speed can be posed in terms of increased surface roughness parameter and increased displacement height. The reduction of solar radiation reaching the ground surface through the vegetation can be expressed as a linear dependence on the shading factor by neglecting complexities due to varying sun angle.

To minimize the number of parameters, we relate both the influences of shading and wind-speed reduction to the shading factor σ_f according to the format

$$E_{\text{dir}} = E_{\text{soil}}(1 - \sigma_f)\,; \tag{B-2}$$

E_{soil} is the evaporation from the soil in the absence of vegetation as discussed in Section 2.

Transpiration is related to the density of vegetation and the soil moisture content. For the two-layer model, these influences are most simply included with the following formulation for transpiration:

$$E_T = E_P k_v \sigma_f \left[\frac{z_1}{z_2}\, g(\theta_1) + \frac{(z_2 - z_1)}{z_2}\, g(\theta_2)\right][1 - (C^*/S)^n]\,,$$

$$g(\theta) = \begin{cases} 1\,, & \theta > \theta_{\text{ref}}\,, \\ \dfrac{\theta - \theta_{\text{wilt}}}{\theta_{\text{ref}} - \theta_{\text{wilt}}}\,, & \theta_{\text{wilt}} \le \theta \le \theta_{\text{ref}}\,, \\ 0\,, & \theta \le \theta_{\text{wilt}}\,; \end{cases} \tag{B-3}$$

where z_1 is the depth of the upper layer (here 5 cm) and z_2 is the depth of the entire two layers (1 m). We have assumed that the root uptake rate is independent of depth within a given layer. After consulting numerous studies, the wilting point, θ_{wilt}, where root uptake ceases, is assigned a value of 0.12. The parameter θ_{ref} is the soil moisture content at which the soil moisture deficit begins to reduce root uptake and transpiration. θ_{ref} is chosen to be 0.25, which is significantly below the saturation values for most soil types.

C^*, the canopy water content and S, the canopy water capacity, are included to represent reduction of transpiration from surfaces covered by a water film. The coefficient k_v is the plant resistance factor chosen to be 1.0 and σ_f is specified to be 0.7. The product of $k_v\sigma_f$ is similar to the commonly used plant coefficient. The parameter n is chosen to be $\frac{1}{2}$ to be consistent with the interception model discussed below.

Some dewfall occurs in the iterations reported in Section 4. Interception is modelled as

$$\frac{dC^*}{dt} = \sigma_f P - E_C,$$
$$E_C = \sigma_f (C^*/S)^n E_P. \tag{B-4}$$

The storage capacity of the canopy, S, is chosen to be 2 mm. P is the precipitation or dewfall rate. This interception model is similar to that of Rutter *et al.* (1971) except that:

(1) the throughfall parameter is replaced with the closely related expression $1 - \sigma_f$ in order to reduce the number of parameters;

(2) the evaporation factor C^*/S is multiplied by σ_f to account for the asymptotic limit that canopy evaporation vanishes as the canopy vanishes; and

(3) n is chosen to be less than unity to correspond to a finite time for the canopy to dry, following rainfall as modelled in Deardorff (1978).

Based on the work of Leyton *et al.* (1967), a value of $n = \frac{1}{2}$ is inferred, which is somewhat less than the $n = \frac{2}{3}$ value chosen by Deardorff (1978).

Once the canopy is saturated ($C^* = S$), all additional rainfall is assumed to fall through to the ground. This is analogous to assuming that drip processes occur instantaneously so that the canopy is never temporarily 'supersaturated'.

References

Al Nakshabandi, G. and Kohnke, H.: 1965, 'Thermal Conductivity and Diffusivity of Soils as Related to Moisture Tension and Other Physical Properties', *Agric. Meteorol.* **2**, 271–279.

Brenner, S., Yang, C.-H., and Mitchell, K.: 1984, *The AFGL Global Spectral Model: Expanded Resolution Baseline Version*, Report No. AFGL–TR–84–0308, 72 pp. [Air Force Geophysics Laboratory/LYP, Hascom AFB, MA 01731, U.S.A.].

Clapp, R. B. and Hornberger, G. M.: 1978, 'Empirical Equations for Some Soil Hydraulic Properties', *Water Resources Res.* **14**, 601–604.

Deardorff, J.: 1978, 'Efficient Prediction of Ground Surface Temperature and Moisture with Inclusion of a Layer of Vegetation', *J. Geophys. Res.* **83**, 1889–1903.

DeBruin, H. A. R.: 1983, 'A Model for the Priestly–Taylor Parameter α', *J. Cli. Appl. Meteorol.* **22**, 572–578.

DeVries, D. A.: 1975, 'Heat Transfer in Soils', in D. A. DeVries and N. H. Afgan (eds.), *Heat and Mass Transfer in the Biosphere*, Scripta Book Co., Washington, D.C., pp. 5–28.

Holtslag, A. A. M. and Van Ulden, A. P.: 1983, 'A Simple Scheme for Daytime Estimates of Surface Fluxes from Routine Weather Data', *J. Cli. Appl. Meteorol.* **22**, 517–529.

Hunt, B. G.: 'A Model Study of Some Aspects of Soil Hydrology Relevant to Climatic Modelling', *Quart. J. R. Meteorol. Soc.* **111**, 1071–1085.

Leyton, L., Reynolds, E. R. C., and Thompson, F. B.: 1967, 'Rainfall Interception in Forest and Moorland', in W. E. Sopper and H. W. Lull (eds.), *Forest Hydrology*, Pergamon, Oxford, pp. 163–178.

Mahrt, L.: 1976, 'Mixed Layer Moisture Structure', *Mon. Wea. Rev.* **104**, 1403–1407.

Mahrt, L. and Ek, M.: 1984, 'The Influence of Atmospheric Stability on Potential Evaporation', *J. Cli. Appl. Meteorol.* **23**, 222–234.

Mahrt, L., and Pan, H.-L.: 1984, 'A Two-Layer Model of Soil Hydrology', *Boundary-Layer Meteorol.* **29**, 1–20.

McCumber, M. C. and Pielke, R. A.: 1981, 'Simulation of the Effects of Surface Fluxes of Heat and Moisture in a Mesoscale Numerical Model Soil Layer', *J. Geophys. Res.* **86**, 9929–9938.

McNaughton, J. L.: 1976, 'Evaporation and Advection. I. Evaporation from Extensive Homogeneous Surfaces', *Quart. J. Roy. Meteorol. Soc.* **102**, 181–191.

Oke, T.: 1978, *Boundary Layer Climates*, Methuen, London, 372 pp.

Rutter, A. J., Kershaw, K. A., Robins, P. C., and Morton, A. J.: 1971, 'A Predictive Model of Rainfall Interception in Forests, 1. Derivation of the Model From a Plantation of Corsican Pine', *Agric. Meteorol.* **9**, 367–384.

Troen, I. and Mahrt, L.: 1986, 'A Simple Model of the Boundary Layer: Sensitivity to Surface Evaporation', *Boundary-Layer Meteorol.* **37**, 129–148.

Van Bavel, C. H. M. and Hillel, D. I.: 1976, 'Calculating Potential and Actual Evaporation from a Bare-Soil Surface by Simulation of Concurrent Flow of Water and Heat', *Agric. Meteorol.* **17**, 453–476.